International Journal of Heat and Mass Transfer 56 (2013) 35–44

Contents lists available at SciVerse ScienceDirect

International Journal of Heat and Mass Transfer

journal homepage: www.elsevier.com/locate/ijhmt

An investigation of natural convection in parallel square plates with a heated bottom surface by an absorbing boundary condition

Wu-Shung Fu *, Wei-Hsiang Wang, Chung-Gang Li, Shang-Hao Huang

Department of Mechanical Engineering, National Chiao Tung University, Hsinchu 30010, Taiwan, ROC

ARTICLE INFO

Article history:
Received 11 May 2012
Received in revised form 24 August 2012
Accepted 30 August 2012
Available online 23 October 2012

Keywords:
Natural convection
Non-reflecting boundary condition
Absorbing boundary condition

ABSTRACT

A study of natural convection in three dimensional square plates is investigated numerically. Several open boundaries co-exist in the physical domain, and a non-reflecting boundary condition applied at the aperture is no longer suitable for solving the problem of this study. An absorbing boundary condition is then adopted and modified in the solution processes. Methods of the Roe scheme, preconditioning and dual time stepping matching LSUGS scheme are used to solve a situation of a low speed compressible flow. The geometry of the physical model is the parallel square plates, and the parameter of Rayleigh number is not high, and then phenomena observed are almost symmetrical. The results of the work have good agreements with the experimental results of a previous paper.

1. Introduction

A subject of natural convection in parallel plates is still an important and attractive topic in both fundamental and applicational research. The subject involves problems of multiple open boundaries which demarcate an inside and an outside of a domain and have functions to allow fluids to flow into and out of the domain reasonably and smoothly according to related physical conditions. Therefore, characteristics of the open boundary deeply affect the phenomena of the inside of the domain. From a view point of theoretical analysis, a correct and appropriate treatment of the open boundary becomes a complex and serious topic.

In order to study the problem induced by the open boundary in an incompressible flow problem, a method [1] of addition of an extra region to the original domain is very popularly adopted. A fully developed condition at the edge of the extra region is often accompanied with the usage of the method mentioned above, and approximate results were obtained. Regretfully, in addition to extra analyses due to the addition of the extra region, the method is often used in analyzing an incompressible flow problem. The method has difficulty to solve the existence of the pollution [2] caused by the interference between the pressure wave reflected from the open boundary and flowing fluids when a numerical computation of a compressible flow is conducted. Therefore, a non-reflecting boundary in which the interference mentioned above can be eliminated is held on the open boundary and to solve the problem of the compressible fluid flow. Rudy and Strikwerda [3] proposed a simple non-reflecting boundary and the results were more consistent with realistic situations than those obtained by a method based on a pressure boundary. Poinsot and Lele [2] developed an ingenious method of Navier–Stokes characteristics boundary condition (NSCBC) to treat compressible fluids flowing through open boundaries of the domain and clarify the effect of the method on the behaviors of compressible fluids flowing through the open boundaries of the domain. Polifke et al. [4] modified the linear relaxation term of the NSCBC, and remarkable results of plane acoustic waves of different frequencies being not reflected from the boundaries of the domain were achieved. Available situations of the above literature [2] and [4] are obtained under the large Mach number $M > 3$ of the speed of fluid. Fu and Li [5,6] proposed a modified method of the NSCBC which can be adopted in all speeds of compressible flows. However, sequential methods of the NSCBC are limited in the treatment of the problem of the non-reflecting boundary on the cross section of the open boundary having one normal direction such as the physical model shown in [6]. And these methods have difficulties to solve the domain having neighboring open boundaries which is like parallel square plates shown in Fig. 1 in which planes of *abdc*, *bfhd*, *fegh* and *eacg* have neighboring open boundaries. Related reasons of the non-reflecting boundary being unavailable for the problem having neighboring open boundaries had been pointed out by Yoo et al. [7] and Lodato et al. [8]. When the direction of the fluid flow was not orthogonal to the non-reflecting boundary, transverse terms were produced on the non-reflecting boundary that caused unstable results induced by accumulation of reflection effects in the corner and edge regions of neighboring non-reflecting boundaries to occur. Finally, the results trended to diverge. Therefore, a

* Corresponding author. Address: Department of Mechanical Engineering, National Chiao Tung University, 1001 Ta Hsueh Road, Hsinchu 30056, Taiwan. Tel.: +886 3 5712121x55110; fax: +886 3 5735065.
E-mail address: wsfu@mail.nctu.edu.tw (W.-S. Fu).

0017-9310/$ - see front matter © 2012 Elsevier Ltd. All rights reserved.
http://dx.doi.org/10.1016/j.ijheatmasstransfer.2012.08.061

Nomenclature

A	area (m^2)
c	speed of sound (m/s)
e	internal energy (J/kg)
e_{target}	target internal energy (J/kg)
g	acceleration of gravity (m/s^2)
k	thermal conductivity (W/mK)
k_0	surrounding thermal conductivity (W/mK)
l_1	width of square plate (m)
l_2	height between square plates (m)
l_3	width of artificial buffer zone (m)
Nu	local Nusselt number defined in Eq. (45) $Nu = \frac{l_2}{k_0(T_H-T_0)}\left[k(T)\frac{\partial T}{\partial y}\right]$
$\overline{Nu}$	averaged Nusselt number defined in Eq. (47) $\overline{Nu} = \frac{1}{A\cdot t}\int_A\int_t \frac{l_2}{k_0(T_H-T_0)}\left[k(T)\frac{\partial T}{\partial y}\right]dtdA$
$\overline{Nu_A}$	area averaged Nusselt number defined in Eq. (46) $\overline{Nu_A} = \frac{1}{A}\int_A \frac{l_2}{k_0(T_H-T_0)}\left[k(T)\frac{\partial T}{\partial y}\right]dA$
P	pressure (Pa)
P_0	surrounding pressure (Pa)
Pr	Prandtl number (ν/α)
R	gas constant (J/kg/K)
Ra	Rayleigh number defined in Eq. (43). $Ra = Pr\frac{g\rho_0^2(T_H-T_0)l_2^3}{T_0\mu(T)^2}$
Ra^*	modified Rayleigh number defined in Eq. (44). $Ra^* = Ra\times\frac{l_2}{l_2}$
T	temperature (K)
T_0	temperature of surroundings (K)
T_H	temperature of heat surface (K)
t	time (s)
u, v, w	velocities in x, y and z directions (m/s)
u_{target}, v_{target}, w_{target}	target velocities in x, y and z directions (m/s)
w_x, w_y, w_z	lengths of artificial buffer zones in x, y and z directions (m)
x, y, z	Cartesian coordinates (m)
X, Z	dimensionless Cartesian coordinates, $\frac{x}{l_1}$ and $\frac{z}{l_1}$

Greek symbols

α	thermal diffusivity rate (m^2/s)
ρ	density (kg/m^3)
ρ_0	surrounding density (kg/m^3)
μ	viscosity (N s/m^2)
μ_0	surrounding viscosity (N s/m^2)
γ	specific heat ratio

method of an absorbing boundary was proposed to solve the domain of the problem including several neighboring open boundaries. In the method used by adding an absorbing boundary, an artificial buffer zone is necessarily added to the original domain. In the artificial buffer zone, two new terms of artificial convection and damping terms are additionally added to the original governing equations to eliminate the reflection of pressure wave from the edge of the artificial buffer zone.

The basic theory of the absorbing boundary is mainly divided into two parts of the perfectly matched layer (PML) and zonal

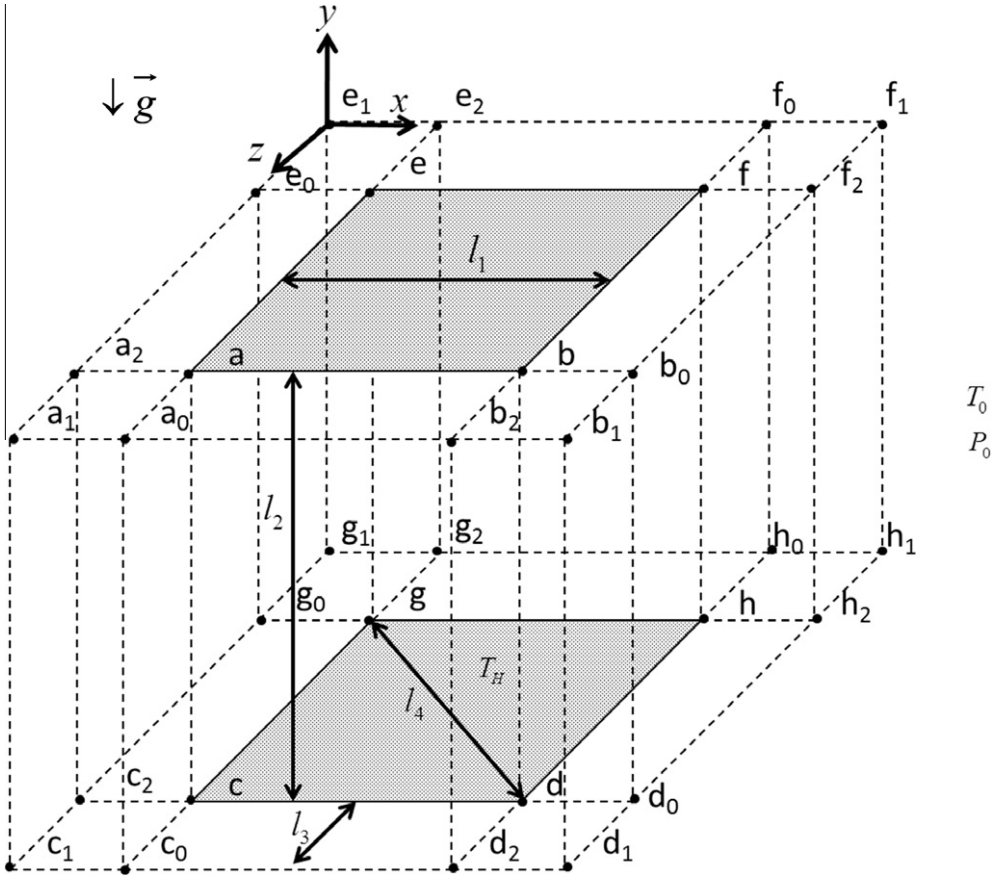

Fig. 1. Physical model of three dimensional parallel square plates.

boundary. The PML was originally proposed by Berenger [9] to solve the Maxwell equation and led electromagnetic waves of different frequencies and incident angles to penetrate an absorbing layer without reflection. Also, the PML was broadly applied to the research of computational electromagnetics. In addition to the extension of application of the PML [10,11], Hu [12] also modified the PML for solving the Euler equation, but it was limited in inviscid fluid flow problems. In order to match the demand of the neighboring open boundaries for viscous fluid flow problems, the zonal boundary in which an artificial buffer zone was added to the original domain was then proposed by Ta'asan and Nark [13] and Wasistho et al. [14]. The method of the zonal boundary mainly adopted the artificial convection and damping terms to eliminate the reflection pressure wave and decay the disturbances. Freund [15] integrated the related theories proposed by Ta'asan and Nark [13] and Wasistho et al. [14] and newly proposed an absorbing layer to substitute the PML method mentioned above to solve problems in viscous fluid flow situations. And the absorbing layer is successfully used to solve one dimensional compressible Navier–Stokes equations indicated in the literature [15]. Based upon the theory of [15], Fu and Li [16] modified the absorbing layer for treating a two dimensional open boundary problem and applied it to solve a two dimensional compressible flow problem with the open boundaries. However, when the modified method [16] was used to apply to a three dimensional open boundary problem, it is rather difficult to determine correct directions of the artificial convection and damping terms in the intersection zone such as a rectangular cubic zone shown in Fig. 1 of which the top and bottom surfaces are $bb_2b_1b_0$ and $dd_2d_1d_0$, respectively. Consequently, the problem of fluids flowing through plates with a three dimensional open boundary, which is one of the most realistic and important problems for industrial applications, is still not clarified yet. A subject of natural convection in parallel square plates is just a problem which is consistent with the problem mentioned above.

Therefore, the study aims to develop a new available method to solve natural convection of parallel square plates with a heated bottom surface numerically. The modified method holds the absorbing boundaries on the open boundaries. In this method the artificial convection and damping terms in the artificial buffer zone are used to avoid reflection phenomena occurring on the open boundaries. Methods of the Roe scheme, preconditioning and dual time stepping are combined and used simultaneously for solving governing equations of the compressible flow induced by a high temperature difference. The results show that the largest magnitude of fluid velocity flowing into parallel squares is observed at the center region of the bottom surface edge, and the largest magnitude of the local Nusselt number is found to be close to the corner region of the bottom surface.

2. Physical model

A physical model of three dimensional parallel square plates mentioned above is indicated in Fig. 1. The three dimensional parallel square plates regarded as an original domain are composed of the top surface of *abfe* and bottom surface of *cdhg*. Open boundaries of the original domain are *bfhd*, *fegh*, *eacg* and *abdc*. The length of the square plate is l_1 and the height between the two squares is l_2. The temperature of the heated bottom square is T_H, and the top square is adiabatic. The direction of gravity is the negative y direction. Since the absorbing boundary is used, an additional zone called an artificial buffer zone is necessarily added to the original domain and indicated by dashed lines in Fig. 1. In this physical model, the direction of the normal line of the artificial buffer zone, in which the surface of $b_2b_1f_1f_0$ is the top surface and the surface of $d_2d_1h_1h_0$ is the bottom surface, directs in the positive x direction. Similarly, the other three artificial buffer zones can be defined, and the three directions of the normal lines of the artificial buffer zones are the negative x direction and the positive and negative z directions, respectively. However, an intersection artificial buffer zone of neighboring artificial buffer zones can be observed at each corner such as a cubic rectangle composed of the top surface of $bb_0b_1b_2$ and the bottom surface of $dd_0d_1d_2$. The intersection artificial buffer zone includes two artificial buffer zones which have different directions of normal lines mentioned above, and the phenomena in the intersection buffer zone are naturally different from those in the artificial buffer zone described earlier. The solution methods used in the true zone are then different. Therefore, the artificial buffer zone should exclude the intersection artificial buffer zone, and the residual zone, in which the surface of bff_2b_0 is the top surface and the surface of dhh_2d_0 is the bottom surface for example, is exclusively called by the artificial buffer zone afterwards. The distance between the boundaries of the original domain and artificial buffer zones is l_3. The temperature and pressure outside the artificial buffer zone are $T_0 = 300$ K and $P_0 = 1$ atm, respectively.

For facilitating the analysis, the following assumptions are made:

1. The flow is laminar flow.
2. The work fluid is ideal gas and follows the equation of state of ideal gas.
3. Velocities on the walls satisfy no slip condition.

The governing equations described in the original domain in which the parameters of viscosity and compressibility of the fluid and gravity are considered simultaneously are shown in the following equations.

$$\frac{\partial U}{\partial t}+\frac{\partial F}{\partial x}+\frac{\partial G}{\partial y}+\frac{\partial H}{\partial z}=S \tag{1}$$

$$P=\rho RT \tag{2}$$

Contents of U,F,G,H and S are separately indicated as follows:

$$\left.\begin{aligned}
U&=\begin{pmatrix}\rho\\ \rho u\\ \rho v\\ \rho w\\ \rho E\end{pmatrix}\\
F&=\begin{pmatrix}\rho u\\ \rho u^2+P-\tau_{xx}\\ \rho uv-\tau_{xy}\\ \rho uw-\tau_{xz}\\ \rho Eu+Pu-k\frac{\partial T}{\partial x}-u\tau_{xx}-v\tau_{xy}-w\tau_{xz}\end{pmatrix}\\
G&=\begin{pmatrix}\rho v\\ \rho u-\tau_{yx}\\ \rho v^2+P-\tau_{yy}\\ \rho vw-\tau_{yz}\\ \rho Ev+Pv-k\frac{\partial T}{\partial y}-u\tau_{yx}-v\tau_{yy}-w\tau_{yz}\end{pmatrix}\\
H&=\begin{pmatrix}\rho w\\ \rho u-\tau_{zx}\\ \rho v-\tau_{zy}\\ \rho vw+P-\tau_{zz}\\ \rho Ew+Pw-k\frac{\partial T}{\partial z}-u\tau_{zx}-v\tau_{zy}-w\tau_{zz}\end{pmatrix}\\
S&=\begin{pmatrix}0\\ 0\\ -(\rho-\rho_0)g\\ 0\\ -(\rho-\rho_0)gv\end{pmatrix}
\end{aligned}\right\} \tag{3}$$

The viscosity and thermal conductivity of the fluid are based upon Sutherland's law and shown as follows:

$$\left.\begin{aligned}&\mu(\mathrm{T}) = \mu_0\left(\tfrac{\mathrm{T}}{\mathrm{T}_0}\right)^{\frac{2}{3}}\tfrac{T_0+110}{T+110}\\&k(T) = \tfrac{\mu(T)\gamma R}{(\gamma-1)Pr}\\&E = \tfrac{P}{\rho(\gamma-1)}+\tfrac{1}{2}(u^2+v^2+w^2)\end{aligned}\right\} \tag{4}$$

where $\rho_0 = 1.1842\ \mathrm{kg/m^3}$, $g = 9.81\ \mathrm{m/s^2}$, $\mu_0 = 1.85\times10^{-5}\ \mathrm{Ns/m^2}$, $\gamma = 1.4$, $R = 287\ \mathrm{J/kg/K}$ and $Pr = 0.72$.

As for the governing equations described in the artificial buffer zone [15], the artificial convection and damping terms are newly adopted. The function of the artificial convection term mainly accelerates outward velocities of fluids via the artificial buffer zone to reach a high speed which almost reaches a supersonic speed at the edge of the artificial buffer zone. And the function of the artificial damping term eliminates the disturbances in the artificial buffer zone. Then general forms of the governing equations in the artificial buffer zone can be described as Eq. (5). Since Eq. (5) is exclusively adopted in the artificial buffer zones, the source term induced by gravity does not exist that is different from Eq. (3) in the original domain

$$\frac{\partial U}{\partial t}+\frac{\partial \widetilde{F}}{\partial x}+\frac{\partial \widetilde{G}}{\partial y}+\frac{\partial \widetilde{H}}{\partial z}+\tilde{\sigma}=0 \tag{5}$$

where

$$\left.\begin{aligned}&\widetilde{F}=F+\tilde{\eta}_F,\tilde{\eta}_F=\begin{Bmatrix}\eta_x\rho\\ \eta_x\rho u\\ \eta_x\rho v\\ \eta_x\rho w\\ \eta_x\rho E\end{Bmatrix}\\&\widetilde{G}=G+\tilde{\eta}_G,\tilde{\eta}_G=\begin{Bmatrix}\eta_y\rho\\ \eta_y\rho u\\ \eta_y\rho v\\ \eta_y\rho w\\ \eta_y\rho E\end{Bmatrix}\\&\widetilde{H}=H+\tilde{\eta}_H,\tilde{\eta}_H=\begin{Bmatrix}\eta_z\rho\\ \eta_z\rho u\\ \eta_z\rho v\\ \eta_z\rho w\\ \eta_z\rho E\end{Bmatrix}\end{aligned}\right\} \tag{6}$$

and

$$\begin{aligned}\tilde{\sigma}=\tilde{\sigma}_x+\tilde{\sigma}_y+\tilde{\sigma}_z=&\begin{bmatrix}\sigma_x(\rho-\rho_{\mathrm{target}})\\ \sigma_x(\rho u-\rho u_{\mathrm{target}})\\ \sigma_x(\rho v-\rho v_{\mathrm{target}})\\ \sigma_x(\rho w-\rho w_{\mathrm{target}})\\ \sigma_x(e-e_{\mathrm{target}})\end{bmatrix}+\begin{bmatrix}\sigma_y(\rho-\rho_{\mathrm{target}})\\ \sigma_y(\rho u-\rho u_{\mathrm{target}})\\ \sigma_y(\rho v-\rho v_{\mathrm{target}})\\ \sigma_y(\rho w-\rho w_{\mathrm{target}})\\ \sigma_y(e-e_{\mathrm{target}})\end{bmatrix}\\&+\begin{bmatrix}\sigma_z(\rho-\rho_{\mathrm{target}})\\ \sigma_z(\rho u-\rho u_{\mathrm{target}})\\ \sigma_z(\rho v-\rho v_{\mathrm{target}})\\ \sigma_z(\rho w-\rho w_{\mathrm{target}})\\ \sigma_z(e-e_{\mathrm{target}})\end{bmatrix}\end{aligned} \tag{7}$$

$\tilde{\eta}_F$, $\tilde{\eta}_G$ and $\tilde{\eta}_H$ are artificial convection terms, and $\tilde{\sigma}_x$, $\tilde{\sigma}_y$ and $\tilde{\sigma}_z$ are artificial damping terms. η_x, η_y and η_z included in $\tilde{\eta}_F$, $\tilde{\eta}_G$ and $\tilde{\eta}_H$ are separately shown as follows:

$$\eta_x=\begin{cases}\eta_{x0l}\left(\frac{w_{xl}-x}{w_{xl}}\right)^{\beta_{xl}} & 0\leqslant x<w_{xl}\\ 0 & w_{xl}\leqslant x<x_{\max}-w_{xr}\\ \eta_{x0r}\left[\frac{x-(x_{\max}-w_{xr})}{w_{xr}}\right]^{\beta_{xr}} & x_{\max}-w_{xr}\leqslant x<x_{\max}\end{cases} \tag{8}$$

$$\eta_y=\begin{cases}\eta_{y0l}\left(\frac{w_{yl}-y}{w_{yl}}\right)^{\beta_{yl}} & 0\leqslant y<w_{yl}\\ 0 & w_{yl}\leqslant y<y_{\max}-w_{yr}\\ \eta_{y0r}\left[\frac{y-(y_{\max}-w_{yr})}{w_{yr}}\right]^{\beta_{yr}} & y_{\max}-w_{yr}\leqslant y<y_{\max}\end{cases} \tag{9}$$

$$\eta_z=\begin{cases}\eta_{z0l}\left(\frac{w_{zl}-z}{w_{zl}}\right)^{\beta_{zl}} & 0\leqslant z<w_{zl}\\ 0 & w_{zl}\leqslant z<z_{\max}-w_{zr}\\ \eta_{z0r}\left[\frac{z-(z_{\max}-w_{zr})}{w_{zr}}\right]^{\beta_{zr}} & z_{\max}-w_{zr}\leqslant z<z_{\max}\end{cases} \tag{10}$$

η_{x0}, η_{y0} and η_{z0} are the target velocities at the edges of the artificial buffer zones. σ_x, σ_y and σ_z are the artificial damping functions and shown as follows:

$$\sigma_x=\begin{cases}\sigma_{x0l}\left(\frac{w_{xl}-x}{w_{xl}}\right)^{\beta_{xl}} & 0\leqslant x<w_{xl}\\ 0 & w_{xl}\leqslant x<x_{\max}-w_{xr}\\ \sigma_{x0r}\left[\frac{x-(x_{\max}-w_{xr})}{w_{xr}}\right]^{\beta_{xr}} & x_{\max}-w_{xr}\leqslant x<x_{\max}\end{cases} \tag{11}$$

$$\sigma_y=\begin{cases}\sigma_{y0l}\left(\frac{w_{yl}-x}{w_{yl}}\right)^{\beta_{yl}} & 0\leqslant y<w_{yl}\\ 0 & w_{yl}\leqslant y<y_{\max}-w_{yr}\\ \sigma_{y0r}\left[\frac{y-(x_{\max}-w_{yr})}{w_{yr}}\right]^{\beta_{yr}} & y_{\max}-w_{yr}\leqslant y<y_{\max}\end{cases} \tag{12}$$

$$\sigma_z=\begin{cases}\sigma_{z0l}\left(\frac{w_{zl}-x}{w_{zl}}\right)^{\beta_{zl}} & 0\leqslant z<w_{zl}\\ 0 & w_{zl}\leqslant z<z_{\max}-w_{zr}\\ \sigma_{z0r}\left[\frac{z-(x_{\max}-w_{zr})}{w_{zr}}\right]^{\beta_{zr}} & z_{\max}-w_{zr}\leqslant z<z_{\max}\end{cases} \tag{13}$$

σ_{x0}, σ_{y0} and σ_{z0} are the target damping functions at the edges of the artificial buffer zones.

Locations of ϕ_0 and $\phi_{\max}$ and length of $w_{\phi l}$ and $w_{\phi r}$ are indicated in Fig. 2. In order to balance the order of the acoustic wave speed and both orders of the target velocities of the artificial convection terms (Eqs. (8)–(10)) and the target damping functions of the artificial damping terms (Eqs. (11)–(13)), the process proposed by Dennis et al. [17] is executed and the order of an original acoustic wave speed is transformed into the similar order of a modified acoustic wave speed. Then new target velocities of the artificial convection terms and new target damping functions of the artificial damping terms are expressed as follows, respectively, and can be adopted in a low speed compressible flow situation

$$\eta_{xo}=c_F\frac{\sqrt{u^2(\Theta-1)^2+4\Theta c^2}}{2} \tag{14}$$

$$\eta_{yo}=c_G\frac{\sqrt{v^2(\Theta-1)^2+4\Theta c^2}}{2} \tag{15}$$

$$\eta_{zo}=c_H\frac{\sqrt{w^2(\Theta-1)^2+4\Theta c^2}}{2} \tag{16}$$

$$\sigma_{xo}=c_x\frac{\sqrt{u^2(\Theta-1)^2+4\Theta c^2}}{2} \tag{17}$$

$$\sigma_{yo}=c_y\frac{\sqrt{v^2(\Theta-1)^2+4\Theta c^2}}{2} \tag{18}$$

$$\sigma_{zo}=c_z\frac{\sqrt{w^2(\Theta-1)^2+4\Theta c^2}}{2} \tag{19}$$

where $\Theta\approx100M^2$ and c is the speed of the sound.

From the previous study [16], the appropriate values of c_F, c_G, c_H, c_x, c_y, c_z are $c_F = c_G = c_H = 1.15$, $c_x = c_y = c_z = 0.05$, and $\beta = 3$, respectively.

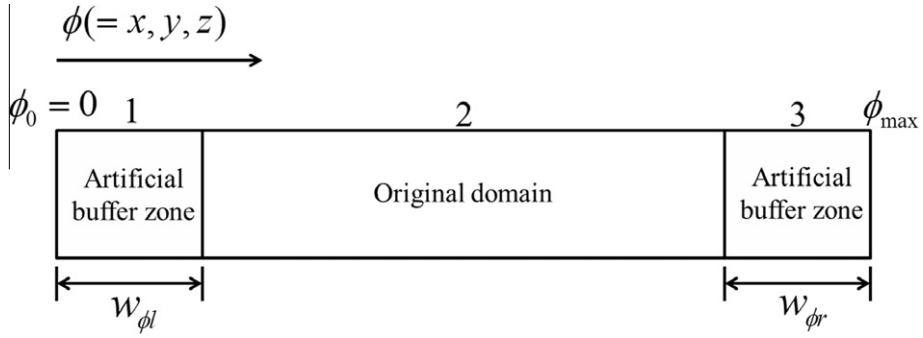

Fig. 2. A diagram of one dimensional absorbing boundary condition.

Thus the magnitudes of the artificial convection terms will be equal to zero at the interface of the original domain and artificial buffer zones and equal to the modified acoustic wave speed at the edges of the artificial buffer zones. And the disturbances of the flowing fluids are gradually reduced to zero accompanied with the location close to the edge of the artificial buffer zone.

3. Numerical method

In natural convection, the speed of the compressible fluid flow is much slower than that of the acoustic wave. The Roe Scheme [18] coordinating the preconditioning method are then adopted to resolve the governing equations shown in Eq. (1) which can be derived as the following equation and shown in Eq. (20)

$$\Gamma\frac{\partial U_p}{\partial\tau}+\frac{\partial F}{\partial x}+\frac{\partial G}{\partial y}+\frac{\partial H}{\partial z}=S \tag{20}$$

where Γ is the preconditioning matrix proposed by Weiss and Smith [19] and U_p is the primitive form of $[P,u,v,w,T]^t$.

The method of dual time stepping is added to calculate the transient state of the physical model. The derived equation is shown in Eq. (21)

$$\Gamma\frac{\partial U_p}{\partial\tau}+\frac{\partial U}{\partial t}+\frac{\partial F}{\partial x}+\frac{\partial G}{\partial y}+\frac{\partial H}{\partial z}=S \tag{21}$$

where τ is an artificial time, t is a physical time and U_p is the primitive form of $[\rho,\rho u,\rho v,\rho w,\rho e]^T$.

When the discretization of Eq. (21) is executed, terms of $\frac{\partial U_p}{\partial\tau}$ and $\frac{\partial U}{\partial t}$ are differentiated by a first-order forward difference and a second-order backward difference, respectively, and terms of $\frac{\partial F}{\partial x}$, $\frac{\partial G}{\partial y}$, and $\frac{\partial H}{\partial z}$ are differentiated by a central difference, the following equation can be obtained

$$\Gamma\frac{U_p^{k+1}-U_p^k}{\Delta\tau}+\frac{3U^{n+1}-4U^n+U^{n-1}}{2\Delta t}+\frac{1}{\Delta x}\left(F^{k+1}_{i+\frac{1}{2},j,k}-F^{k+1}_{i-\frac{1}{2},j,k}\right)+\frac{1}{\Delta y}\left(G^{k+1}_{i,j+\frac{1}{2},k}-G^{k+1}_{i,j-\frac{1}{2},k}\right)+\frac{1}{\Delta z}\left(H^{k+1}_{i,j,k+\frac{1}{2}}-H^{k+1}_{i,j,k-\frac{1}{2}}\right)=S \tag{22}$$

The terms of U^{k+1} and F^{k+1} in Eq. (22) are necessary to be linearized and expressed as follows:

$$U^{k+1}=U^k+M\Delta U_p \tag{23}$$

in which $M=\frac{\partial U}{\partial U_p}$ and $A_p=\frac{\partial F^k}{\partial U_p}$

$$F^{k+1}=F^k+A_p\Delta U_p \tag{24}$$

Where $A_p=\frac{\partial F}{\partial U_p}$ is the flux jacobian and the same methods for $B_p=\frac{\partial G}{\partial U_p}$ and $C_p=\frac{\partial H}{\partial U_p}$ are used in linearization of G^{k+1} and H^{k+1}, respectively.

Eqs. (23) and (24) are substituted into Eq. (22), the following equation is derived

$$\left[\frac{I}{\Delta\tau}+\Gamma^{-1}M\frac{3}{2\Delta t}+\Gamma^{-1}\left(\delta_xA_p^k+\delta_yB_p^k+\delta_zC_p^k\right)\right]\Delta U_p=\Gamma^{-1}R^k \tag{25}$$

where δ_x, δ_y, and δ_z are central-difference operators and $R^k=S-\left(\frac{3U^k-4U^n+U^{n-1}}{2\Delta t}\right)-(\delta_xF^k+\delta_yG^k+\delta_zH^k)$.

The solver of Eq. (26) is the LUSGS implicit method proposed by Yoon and Jameson [20]

$$\begin{aligned}A_p&=\Gamma^{-1}A_p^k\\B_p&=\Gamma^{-1}B_p^k\\C_p&=\Gamma^{-1}C_p^k\end{aligned} \tag{26}$$

Eq. (25) can be rearranged as follows:

$$(L+D+U)\Delta U_p=\Gamma^{-1}R^k \tag{27}$$

where

$$\left.\begin{aligned}L&=-\left[\tfrac{1}{\Delta x}\left(A_p^+\right)_{i-1,j,k}+\tfrac{1}{\Delta y}\left(B_p^+\right)_{i,j-1,k}+\tfrac{1}{\Delta z}\left(C_p^+\right)_{i,j,k-1}\right]\\D&=\tfrac{I}{\Delta\tau}+\Gamma^{-1}M\tfrac{3}{2\Delta t}+\left\{\tfrac{1}{\Delta x}\left[\left(A_p^+\right)_{i,j,k}-\left(A_p^-\right)_{i,j,k}\right]+\tfrac{1}{\Delta y}\left[\left(B_p^+\right)_{i,j,k}-\left(B_p^-\right)_{i,j,k}\right]+\tfrac{1}{\Delta z}\left[\left(C_p^+\right)_{i,j,k}-\left(C_p^-\right)_{i,j,k}\right]\right\}\\U&=\left[\tfrac{1}{\Delta x}\left(A_p^-\right)_{i+1,j,k}+\tfrac{1}{\Delta y}\left(B_p^-\right)_{i,j+1,k}+\tfrac{1}{\Delta z}\left(C_p^-\right)_{i,j,k+1}\right]\end{aligned}\right\} \tag{28}$$

As for the computation of $R^k=S-\left(\frac{3U^k-4U^n+U^{n-1}}{2\Delta t}\right)-(\delta_xF^k+\delta_yG^k+\delta_zH^k)$ in the right hand side of Eq. (27), the terms in F shown in Eq. (3) can be divided into two parts. One is an inviscid term F_{inviscid} and the other is a viscous term F_{viscid}

$$F_{\text{inviscid}}=\begin{pmatrix}\rho u\\ \rho u^2+P\\ \rho uv\\ \rho uw\\ \rho Eu+Pu\end{pmatrix} \tag{29}$$

$$F_{\text{viscous}}=\begin{pmatrix}0\\ -\tau_{xx}\\ -\tau_{xy}\\ -\tau_{xz}\\ -k\frac{\partial T}{\partial x}-u\tau_{xx}-v\tau_{xy}-w\tau_{xz}\end{pmatrix} \tag{30}$$

The methods of Roe scheme and preconditioning are utilized to calculate the magnitude of F_{inviscid} at the location of $(i+\frac{1}{2})$ between the cells for a low Mach number condition

$$F_{\text{inviscid},i+\frac{1}{2}}=\frac{1}{2}(F_R+F_L)-\frac{1}{2}\left\{|\Gamma^{-1}A_p|\Delta U_P\right\} \tag{31}$$

The MUSCL scheme with a third order proposed by Abalakin et al. [21] is used to compute Eq. (31). A forth order central difference is adopted to calculate the F_{viscous}, and Eq. (32) can be obtained

$$\frac{\partial u}{\partial x}=\frac{u_{i-2}-8u_{i-1}+8u_{i+1}-u_{i+2}}{12\Delta x}+o(\Delta x^4) \tag{32}$$

In order to explain the calculation in the artificial buffer zones and the intersection artificial buffer zones mentioned above, a one-dimensional artificial buffer zone shown in Fig. 2 is used to describe the treatment of absorbing boundary conditions. The zones of 1 and 3 are the artificial buffer zones, and the zone of 2 is the original domain w indicates the length of the artificial buffer zone, l and r mean the left and right sides, respectively. ϕ_0 and $\phi_{\max}$ represent the start and end locations of the total domain including the zones of 1, 2 and 3. In order to avoid the reflection of acoustic waves at ϕ_0 and $\phi_{\max}$ rebounding into the zone of 2, the artificial convection term accelerates the velocities of fluids, which are in the zones of 1 and 3 and flow out of the original domain, to be a high speed and greater than the sound speed at edges ϕ_0 and $\phi_{\max}$. The artificial damping term directly multiplies the disturbances of fluid velocities with an appropriate damping function to cause the disturbances to be zero within the artificial buffer zone.

Since phenomena in the artificial buffer zone and the intersection of artificial buffer zones mentioned above are rather different that leads the contents of the artificial convection and damping terms in the governing equations Eq. (4) to be different. Therefore, the governing equations of the artificial buffer zone which is orthogonal to the x direction can be expressed as follows:

$$\left.\begin{aligned}\widetilde{F}&=F+\tilde{\eta}_F,\tilde{\eta}_F=\begin{Bmatrix}\eta_x\rho\\ \eta_x\rho u\\ \eta_x\rho v\\ \eta_x\rho w\\ \eta_x\rho E\end{Bmatrix}\\ \widetilde{G}&=G+\tilde{\eta}_G,\tilde{\eta}_G=0\\ \widetilde{H}&=H+\tilde{\eta}_H,\tilde{\eta}_H=0\end{aligned}\right\} \tag{33}$$

$$\tilde{\sigma}=\tilde{\sigma}_x=\begin{bmatrix}\sigma_x(\rho-\rho_{\text{target}})\\ \sigma_x(\rho u-\rho u_{\text{target}})\\ \sigma_x(\rho v-\rho v_{\text{target}})\\ \sigma_x(\rho w-\rho w_{\text{target}})\\ \sigma_x(e-e_{\text{target}})\end{bmatrix} \tag{34}$$

Governing equations of the artificial buffer zone which is orthogonal to the z direction can be expressed as follows:

$$\left.\begin{aligned}\widetilde{F}&=F+\tilde{\eta}_F,\tilde{\eta}_F=0\\ \widetilde{G}&=G+\tilde{\eta}_G,\tilde{\eta}_G=0\\ \widetilde{H}&=H+\tilde{\eta}_H,\tilde{\eta}_H=\begin{Bmatrix}\eta_z\rho\\ \eta_z\rho u\\ \eta_z\rho v\\ \eta_z\rho w\\ \eta_z\rho E\end{Bmatrix}\end{aligned}\right\} \tag{35}$$

$$\tilde{\sigma}=\tilde{\sigma}_z=\begin{bmatrix}\sigma_z(\rho-\rho_{\text{target}})\\ \sigma_z(\rho u-\rho u_{\text{target}})\\ \sigma_z(\rho v-\rho v_{\text{target}})\\ \sigma_z(\rho w-\rho w_{\text{target}})\\ \sigma_z(e-e_{\text{target}})\end{bmatrix} \tag{36}$$

And governing equations used in intersections of artificial buffer zones can be expressed as follows:

$$\left.\begin{aligned}\widetilde{F}&=F+\tilde{\eta}_F,\tilde{\eta}_F=\begin{Bmatrix}\eta_x\rho\\ \eta_x\rho u\\ \eta_x\rho v\\ \eta_x\rho w\\ \eta_x\rho E\end{Bmatrix}\\ \widetilde{G}&=G+\tilde{\eta}_G,\tilde{\eta}_G=0\\ \widetilde{H}&=H+\tilde{\eta}_H,\tilde{\eta}_H=\begin{Bmatrix}\eta_z\rho\\ \eta_z\rho u\\ \eta_z\rho v\\ \eta_z\rho w\\ \eta_z\rho E\end{Bmatrix}\end{aligned}\right\} \tag{37}$$

$$\tilde{\sigma}=\tilde{\sigma}_x+\tilde{\sigma}_z=\begin{bmatrix}\sigma_x(\rho-\rho_{\text{target}})\\ \sigma_x(\rho u-\rho u_{\text{target}})\\ \sigma_x(\rho v-\rho v_{\text{target}})\\ \sigma_x(\rho w-\rho w_{\text{target}})\\ \sigma_x(e-e_{\text{target}})\end{bmatrix}+\begin{bmatrix}\sigma_z(\rho-\rho_{\text{target}})\\ \sigma_z(\rho u-\rho u_{\text{target}})\\ \sigma_z(\rho v-\rho v_{\text{target}})\\ \sigma_z(\rho w-\rho w_{\text{target}})\\ \sigma_z(e-e_{\text{target}})\end{bmatrix} \tag{38}$$

The direction of the fluid flow of the artificial buffer zone should be outward relative to the original domain, and then in the zone of 1 (Fig. 2) a backward finite difference form is adopted to derive the differential form. It can be expressed as Eq. (39). Similarly, in the zone of 3 (Fig. 2) a forward finite difference form is adopted and it can be expressed as Eq. (40).

For zone of 1

$$\left.\begin{aligned}\eta_\phi\tfrac{\partial\rho}{\partial\phi}&=\eta_\phi\tfrac{\rho_i-\rho_{i+1}}{\Delta\phi}\\ \eta_\phi\tfrac{\partial\rho u}{\partial\phi}&=\eta_\phi\tfrac{\rho u_i-\rho u_{i+1}}{\Delta\phi}\\ \eta_\phi\tfrac{\partial\rho v}{\partial\phi}&=\eta_\phi\tfrac{\rho v_i-\rho v_{i+1}}{\Delta\phi}\\ \eta_\phi\tfrac{\partial\rho w}{\partial\phi}&=\eta_\phi\tfrac{\rho w_i-\rho w_{i+1}}{\Delta\phi}\\ \eta_\phi\tfrac{\partial\rho E}{\partial\phi}&=\eta_\phi\tfrac{\rho E_i-\rho E_{i+1}}{\Delta\phi}\end{aligned}\right\} \tag{39}$$

For zone of 3

$$\left.\begin{aligned}\eta_\phi\tfrac{\partial\rho}{\partial\phi}&=\eta_\phi\tfrac{\rho_i-\rho_{i-1}}{\Delta\phi}\\ \eta_\phi\tfrac{\partial\rho u}{\partial\phi}&=\eta_\phi\tfrac{\rho u_i-\rho u_{i-1}}{\Delta\phi}\\ \eta_\phi\tfrac{\partial\rho v}{\partial\phi}&=\eta_\phi\tfrac{\rho v_i-\rho v_{i-1}}{\Delta\phi}\\ \eta_\phi\tfrac{\partial\rho w}{\partial\phi}&=\eta_\phi\tfrac{\rho w_i-\rho w_{i-1}}{\Delta\phi}\\ \eta_\phi\tfrac{\partial\rho E}{\partial\phi}&=\eta_\phi\tfrac{\rho E_i-\rho E_{i-1}}{\Delta\phi}\end{aligned}\right\} \tag{40}$$

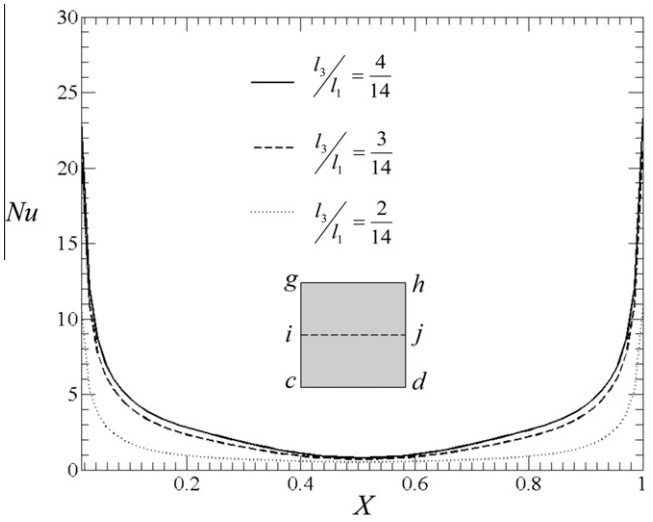

Fig. 3. Distributions of local Nusselt numbers along $\overline{ij}$ of different lengths of the artificial buffer zone under $Ra^* = 1.72 \times 10^5$.

$\phi = x, z$

Eqs. (39) and (40) are adopted for the artificial buffer zones of the directions of x and z, respectively. For the intersection artificial buffer zone, the finite difference derived in the x direction and the finite difference derived in the z direction should be considered simultaneously.

In order to solve the results of the original domain and artificial buffer zone, Eqs. (1) and (5) are combined and the integration of the governing equations can be indicated as follows:

$$\frac{\partial U}{\partial t} + \frac{\partial \widetilde{F}}{\partial x} + \frac{\partial \widetilde{G}}{\partial y} + \frac{\partial \widetilde{H}}{\partial z} + \tilde{\sigma} + S = 0 \tag{41}$$

For the calculation of the original domain, the artificial convection terms and damping terms are equal to zero. Oppositely, for the calculation of the domain of the artificial buffer zone, the source term is equal to zero. Thus a calculation procedure is briefly described as follows:

(1) Assign the initial conditions of pressure, velocity and temperature of the artificial buffer zone, intersection artificial buffer zone and original domain. The temperature of the heated bottom plate is T_H = 700 K.
(2) Use the MUSCL method to calculate Eq. (25) and to obtain the magnitude of ΔU_p.

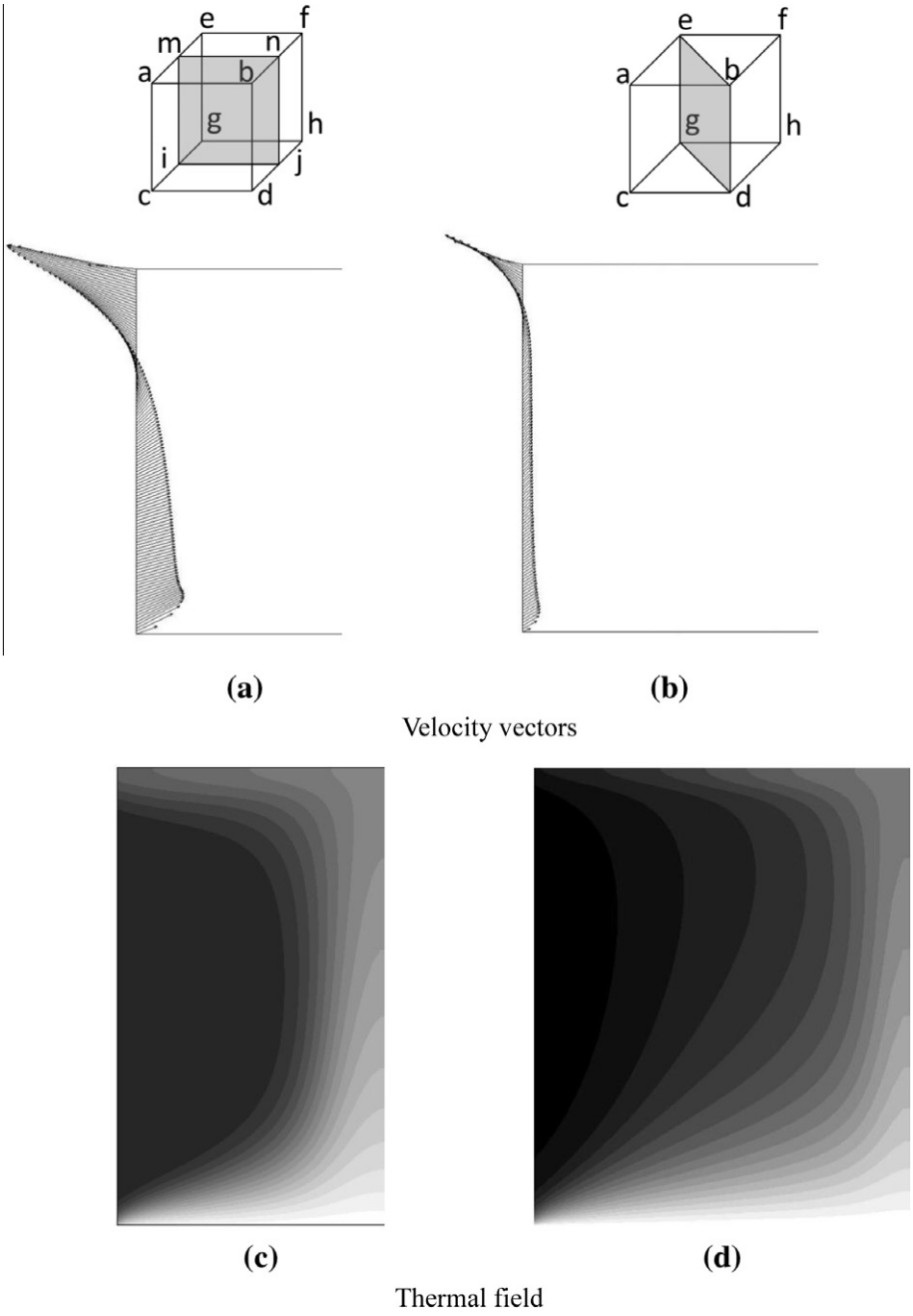

Fig. 4. Distributions of velocity vectors and thermal fields of different cross-sections under $Ra^* = 1.55 \times 10^6$.

(3) Substitute the magnitude of ΔU_p into Eq. (31) and use the Roe scheme to calculate magnitudes of inviscid terms of F_{inviscid}.
(4) Calculate Eq. (32) to obtain magnitudes of viscous terms and substitute into Eqs. (29) and (30).
(5) Solve U_p^{k+1} by the following Eq. (42)

$$U_p^{k+1} = U_p^k + \Delta U_p^k \tag{42}$$

(6) Calculate Eq. (22) and examine the convergence of the computation of U_p^{k+1}. Repeat (2)–(5) until the convergent criteria are satisfied and the convergent magnitude of U_p^{k+1} will be regarded as that of U_p of the $(n+1)$th time step and the process proceeds to the next time step. The convergent criteria of variables are $\frac{\psi^{n+1}-\psi^n}{\psi^{n+1}} < 10^{-3}$, $\psi = p, u, v, w, T$.

4. Results and discussion

The height of parallel square plates is usually regarded as a characteristic length when the Rayleigh number is defined and expressed as follows:

$$Ra = \Pr \frac{g\rho_0^2(T_H - T_0)l_2^3}{T_0\mu(T)^2} \tag{43}$$

However, the area of the heated bottom wall affects heat transfer phenomena remarkably. In order to highlight the influence of the area of the heated wall, the modified Rayleigh number Ra^* is newly defined in the following equation:

$$Ra^* = Ra \times \frac{l_1}{l_2} \tag{44}$$

Besides, the local Nusselt number Nu, the area averaged Nusselt number $\overline{Nu_A}$ and the average Nusselt number $\overline{Nu}$ are defined as follows, respectively

$$Nu = \frac{l_2}{k_0(T_H - T_0)}\left[k(T)\frac{\partial T}{\partial y}\right] \tag{45}$$

$$\overline{Nu_A} = \frac{1}{A}\int_A \frac{l_2}{k_0(T_H - T_0)}\left[k(T)\frac{\partial T}{\partial y}\right]dA \tag{46}$$

$$\overline{Nu} = \frac{1}{A\cdot t}\int_A\int_t \frac{l_2}{k_0(T_H - T_0)}\left[k(T)\frac{\partial T}{\partial y}\right]dtdA \tag{47}$$

In this study, three different magnitudes of Ra^* s are considered, and there are $Ra^* = 1.72\times10^5\left(\frac{l_1}{l_2}=\frac{7}{2}\right)$, $Ra^* = 1.55\times10^6\left(\frac{l_1}{l_2}=\frac{7}{6}\right)$ and $Ra^* = 4.31\times10^6\left(\frac{l_1}{l_2}=\frac{7}{10}\right)$.

In Fig. 3, in order to take care of both accuracy of the width of the artificial buffer zones and computational efficiency, the local Nusselt numbers distributed on the line $\overline{ij}$ of the heated bottom surface with three different ratios of $l_3/l_1 = 2/14$, $l_3/l_1 = 3/14$ and $l_3/l_1 = 4/14$ are indicated, respectively. The computational grids of the original domain are $70\times40\times70$, and the computational grids distributed in the artificial buffer zone are 10, 15 and 20, respectively. The total computational grids are $90\times40\times90$, $100\times40\times100$ and $110\times40\times110$. According to the results, the local Nusselt numbers of $l_3/l_1 = 3/14$ and $l_3/l_1 = 4/14$ cases are more consistent than those of $l_3/l_1 = 2/14$ case. Then the width ratio of $l_3/l_1 = 4/14$ is chosen to calculate the following results.

In Fig. 4a, velocity vectors distributed on the edge of the cross section of *ijnm* are indicated. The longer the velocity vector is, the quicker the velocity is. The bottom surface is heated, then cool fluids are sucked from their surroundings and flow between the parallel square plates along the bottom surface. Due to the effect of the buoyancy force, the cool fluids heated by the bottom surface ascend and impinge on the top surface. Finally, the cooling fluids turn and flow out of the space between the parallel square plates. As a result, the variation of the velocities of the cooling fluids flowing into the plates at the edge of $\overline{im}$ is from quick to slow accompanied with a distance increasing from the bottom surface. At a certain location away from the bottom surface, the velocities of the cooling fluids become zero. Beyond the location shown in the figure, the velocities of the cool fluids turn and are gradually accelerated to flow out of the plates. Near the bottom surface, the velocities of the cool fluids are affected by the buoyancy force, and the velocities of the cool fluids move in a slightly upward direction. The cool fluids flow out of the plates along the top surface after they impinge on the top surface, and then the direction of the velocities of the cool fluids is almost parallel to the top surface.

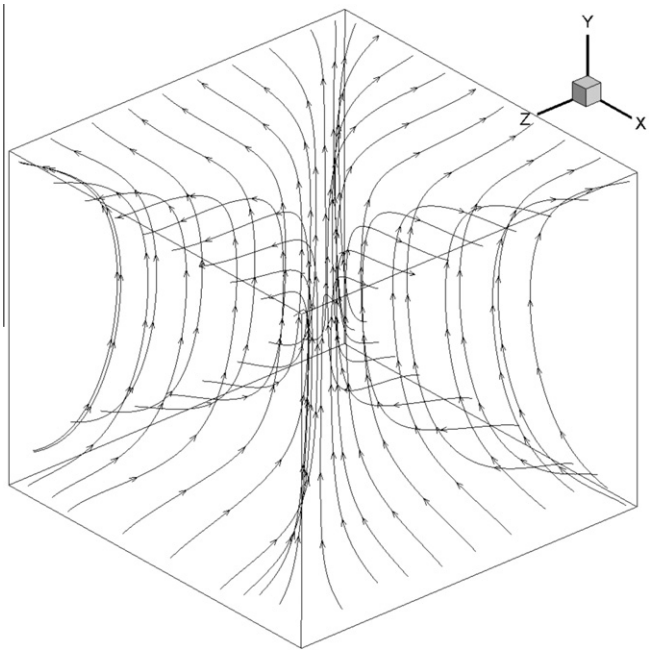

Fig. 5. Distribution of streamlines under $Ra^* = 1.55\times10^6$.

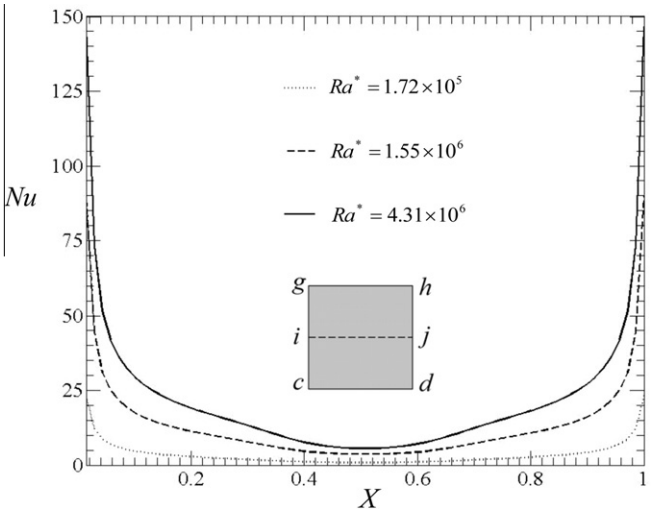

Fig. 6. Distributions of local Nusselt numbers along $\overline{ij}$ under different modified Rayleigh numbers.

In Fig. 4b, velocity vectors distributed on the edge of the diagonal plane of *gdbe* are shown. Since the bottom surface is the square plate, the amount of fluid flows into the plates mainly via edges of $\overline{cd}$, $\overline{dh}$, $\overline{hg}$ and $\overline{gc}$, and the velocity distribution of the amount of fluid on the four edges mentioned above are the same and symmetric. Velocity vectors distributed on $\overline{ge}$ of the diagonal plane are then extruded by those distributed on both sides of *eacg* and *efhg*. Consequently, velocity vectors are smaller than those shown in Fig. 4a.

In Fig. 4c, a thermal field which is the left half side of the cross section of *ijnm* is indicated. The darker the color is, the lower the temperature is. The cooling fluids are gradually heated by the bottom surface from the edge to the center. Then a higher temperature region is concentrated in a central region of the plates. A big dark region beside the central region is observed. The phenomenon means that some cool fluids in the dark region flowing into and out of the plates are just induced by the ascending heated fluids in the central region and not directly heated by the bottom surface.

A thermal field on the left half side of the diagonal cross section is indicated in Fig. 4d. In the central region, the temperatures of the cool fluids heated by the bottom surface increase and lead the cool fluids to ascend to the top surface. This phenomenon naturally causes the thermal field shown in Fig. 4d to be similar to that shown in Fig. 4c.

In Fig. 5, a distribution of streamlines in the parallel square plates is indicated. Based on the diagonal cross section, the streamlines distribute symmetrically. The phenomenon is consistent with natural convection mode.

In Fig. 6, distributions of local Nusselt numbers along $\overline{ij}$ under different modified Rayleigh numbers are shown. Naturally, the larger the Rayleigh number is, the more remarkable heat transfer rate can be achieved. The cool fluids from the outside flow between the plates which leads the magnitudes of the local Nusselt numbers to be decreased from the edge to center of the bottom surface.

In Fig. 7a, a dimensionless parameter *L* means lengths of $\overline{ij}$ and $\overline{gd}$ to be normalized by the length of $\overline{gd}$. The temperatures of the fluids in the central region are higher than those in the other regions which causes the local Nusselt numbers in the central region to be lower than those in the other regions, and the results are displayed in Fig. 7a. Shown in Fig. 7b, local Nusselt numbers distributed on the heated bottom surface are indicated. The darker the color is, the smaller the local Nusselt number is. Heated distances from the center ($L = 0.5$) to the locations of *i* and *j* are shorter than those from the center to the location of *g* and *d*. Consequently, the shape formed by the same local Nusselt numbers is similar to a concave quadrangle.

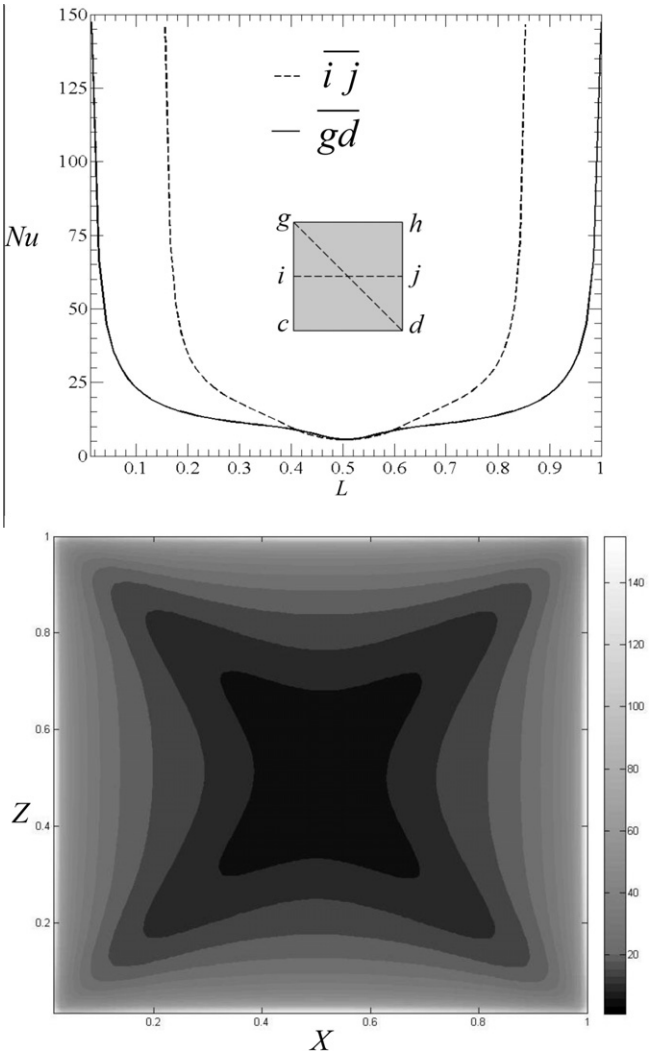

Fig. 7. Distributions of (a) local Nusselt numbers along $\overline{ij}$ and $\overline{gd}$ (b) contour of local Nusselt numbers on the heated bottom surface for $Ra^* = 4.31 \times 10^6$.

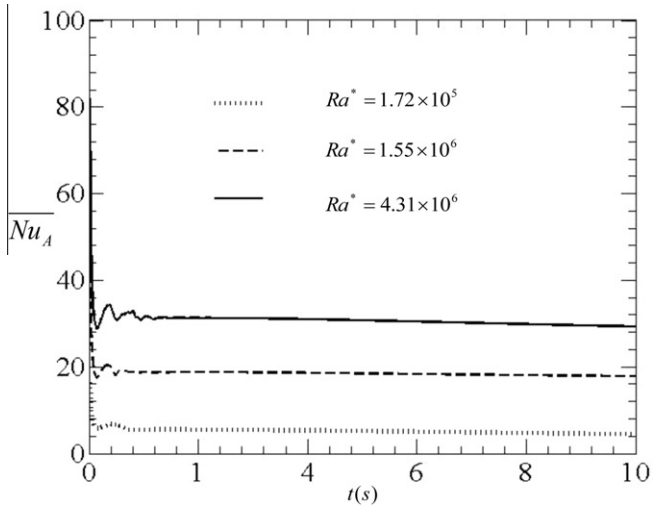

Fig. 8. Distributions of area averaged Nusselt numbers with time under different modified Rayleigh numbers.

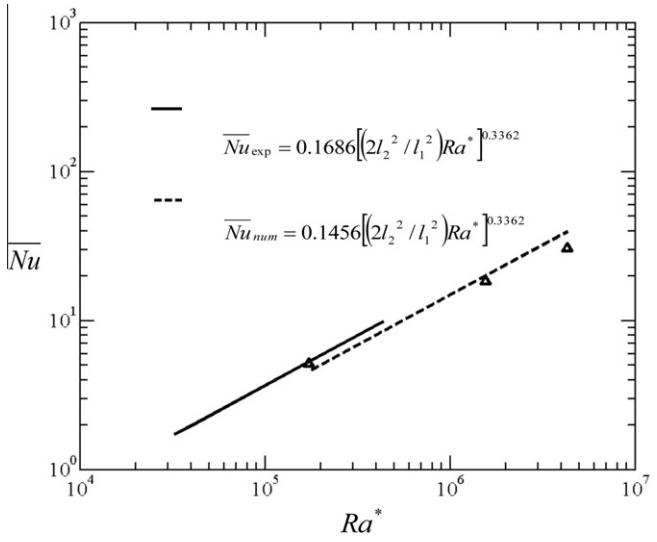

Fig. 9. Comparison of present results and results of Turgut and Onur [22].

In Fig. 8, variations of area averaged Nusselt numbers obtained by three different Rayleigh numbers with time are shown, respectively. Naturally, the larger the Rayleigh number is, the larger the area averaged Nusselt number can be achieved. Except for an early stage of development, the variations of the local Nusselt numbers reveal a steady phenomenon.

Shown in Fig. 9, the results of this work compared with the experimental results of Turgut and Onur [22] are indicated. Main ranges studied by both works have a slight deviation, and in the overlap range both results have good consistency. The maximum error of $\overline{Nu}$ under $Ra^* = 1.72 \times 10^5$ between the present results and existing experimental results is 2.72%.

5. Conclusions

A study of natural convection of fluids moving between parallel squares plates is investigated numerically. Numerical methods of the Roe scheme, preconditioning and dual time stepping are adopted for solving governing equations of a low speed compressible flow. Some conclusions are drawn as follows:

1. The model is parallel square plates, phenomena occurring in the domain are mainly symmetrical. The cool fluids are sucked from their surroundings and heated by the bottom surface and ascend and impinge on the top surface.
2. In order to guarantee the accuracy and economize the computational time, the ratio of the length of the artificial buffer zone to the length of the domain should be validated, in this work the ratio is equal to 4/14.
3. The numerical results of this study have good consistency with the experimental results of the previous study. The method is suitable for solving other three dimensional problems.

Acknowledgement

The authors gratefully acknowledge the support of the Natural Science Council, Taiwan, ROC under Contact NSC99-2221-E-009-058.

References

[1] K. Khanafer, K. Vafai, Effective boundary conditions for buoyancy-driven flows and heat transfer in fully open-ended two-dimensional enclosures, Int. J. Heat Mass Transfer 45 (2002) 2527–2538.
[2] T.J. Poinsot, S.K. Lele, Boundary conditions for direct simulations of compressible viscous flows, J. Comput. Phys. 101 (1992) 104–129.
[3] D.H. Rudy, J.C. Strikwerda, A nonreflecting outflow boundary condition for subsonic Navier–Stokes calculations, J. Comput. Phys. 36 (1980) 55–70.
[4] W. Polifke, C. Wall, P. Moin, Partially reflecting and non-reflecting boundary conditions for simulation of compressible viscous flow, J. Comput. Phys. 202 (2005) 710–736.
[5] Wu-Shung Fu, Chung-Gang Li, Chien-Ping Huang, Jieh-Chau Huang, An investigation of a high temperature difference natural convection in a finite length channel without Bossinesq assumption, Int. J. Heat Mass Transfer 52 (2009) 571–2580.
[6] Wu-Shung Fu, Chung-Gang Li, Tseng Ching-Chi, An investigation of a dual-reflection phenomenon of a natural convection in a three dimensional horizontal channel without Boussinesq assumption, Int. J. Heat Mass Transfer 53 (2010) 575–1585.
[7] C. Yoo, Y. Wang, A. Trouvé, H. Im, Characteristic boundary conditions for direct simulations of turbulent counterflow flams, Combust. Theory Model. 9 (4) (2005) 617–646.
[8] G. Lodato, P. Domingo, L. Vervisch, Three-dimensional boundary conditions for direct and large-eddy simulation of compressible viscous flows, J. Comput. Phys. 227 (2008) 5105–5143.
[9] J.P. Berenger, A perfectly matched layer for the absorption of electromagnetic waves, J. Comput. Phys. 114 (1994) 85–200.
[10] F.Q. Hu, On absorbing boundary conditions of linearized Euler equations by a perfectly matched layer, J. Comput. Phys. 129 (1996) 01–219.
[11] F.Q. Hu, On perfectly matched layer as an absorbing boundary condition, AIAA Paper (1996) 96–1664.
[12] F.Q. Hu, A stable perfectly matched layer for linearized Euler equations in unsplit physical variables, J. Comput. Phys. 173 (2001) 55–480.
[13] S. Ta'asan, D.M. Nark, An absorbing buffer zone technique for acoustic wave propagation, AIAA Aerospace Sciences Meeting and Exhibit (1995).
[14] B. Wasistho, B.J. Geurts, J.G.M. Kuerten, Simulation techniques for spatially evolving instabilities in compressible flow over a flat plate, Comput. Fluids 26 (7) (1997) 13–739.
[15] J.B. Freund, Proposed inflow/outflow boundary condition for direct computation of aerodynamic sound, AIAA 35 (4) (1997) 40–742.
[16] W.S. Fu, C.G. Li, Y. Huang, The Application of CFD in computing aeroacoustics of jet flow's, in: The Seventh International Conference on Flow Dynamics, 2010.
[17] J. Dennis, P. Thomas, B. Pieter, Recent enhancements to overflow, in: 35th Aerospace Sciences Meeting and Exhibit, Reno, NV, 1997.
[18] P.L. Roe, Approximation Riemann solver, parameter vectors, and difference schemes, J. Comput. Phys. 43 (1981) 357–372.
[19] J.M. Weiss, W.A. Simth, Preconditioning applied to variable and constants density flows, AIAA 33 (1995) 2050–2056.
[20] S. Yoon, S. Jameson, Lower-upper symmetric-Gauss-Seidel method for the Euler and Navier–Stokes equations, AIAA 26 (1988) 1025–1026.
[21] I. Abalakin, A. Dervieux, T. Kozubskaya, A vertex centered high order MUSCL scheme applying to linearized Euler acoustics, INRIA (2002). No. 4459.
[22] O. Turgut, N. Onur, An experimental and three-dimensional numerical study of natural convection heat transfer between two horizontal parallel plates, Int. Commun. Heat Mass Transfer 34 (2007) 644–652.